Iranian Journal of Chemical Engineering

Journal Homepage: www.ijche.com

pISSN: 1735-5397
eISSN: 2008-2355

Combination of Machine Learning and Artificial Neural Networks to Predict the Tensile Modulus of Thermoplastic Nanocomposites: The Role of Polymer/Particle Interphase

Reza Mohammadi*[1,2], *Esmail Sharifzadeh*[1,2]

[1]*Department of Chemical Engineering, Faculty of Petroleum and Chemical Engineering, Razi University, Kermanshah, Iran*
[2]*Polymer Research Division, Advanced Chemical Engineering Research Center, Razi University, Kermanshah, Iran*

ARTICLE INFO

Article type:
Research article

Article history:
Received: 2025-11-25
Revised: 2025-12-20
Accepted: 2025-12-25
Available online: 2025-12-30

Keywords:
Nanocomposites,
Tensile modulus,
Artificial neural networks (ANN),
Machine learning,
Interphase

ABSTRACT

Polymer nanocomposites reinforced with multi-walled carbon nanotubes (MWCNTs) offer promising mechanical performance; however, predicting their tensile modulus remains challenging due to the complex interplay of multiple factors such as filler content, functionalization, and interphase quality. In this study, a dataset of 229 samples was compiled from literatures, augmented via cubic spline interpolation to 4,933 training points, and analyzed using six machine learning models, including SVR, Random Forest, Gradient Boosting Regressor, XGBoost, KNN, and Artificial Neural Networks (ANNs). The inclusion of the interphase modulus (E_i), calculated via an extended Ji model, was proved critical for improving prediction accuracy. Among all models, Gradient Boosting Regressor and XGBoost achieved the best predictive performance (Test R^2 = 0.9868 and 0.9837, respectively), while ANN demonstrated competitive accuracy (Test R^2 = 0.9703) but higher sensitivity under cross-validation (Mean CV R^2 = 0.7486). Feature importance analysis using SHAP further confirmed the significant contribution of E_i to prediction outcomes. Overall, this work demonstrates that incorporating physically-informed features like interphase modulus, combined with robust machine learning pipelines, can substantially enhance the predictive modeling of nanocomposite mechanical properties, providing a valuable tool for material design and optimization.

DOI: 10.22034/ijche.2026.562053.1579 URL: https://www.ijche.com/article_239143.html

*Corresponding author: E.sharifzadeh@razi.ac.ir

1. Introduction

Polymers are widely used in industrial and domestic applications due to their low weight, ease of processing, resistance to harsh environments, and cost-effectiveness [1-4]. Their versatility has made them a staple in many engineering systems [5-8]. However, their relatively poor mechanical properties, especially when compared to traditional materials such as metals and ceramics, remain a major limitation [9-12]. One effective way to address this issue is reinforcing the polymer matrix with a secondary phase, particularly at the nanoscale [13-15]. Nanoparticles, because of their high surface-to-volume ratio, interact more efficiently with the polymer matrix than conventional fillers [16-19]. This interaction often leads to the formation of an interphase region, which plays a crucial role in transferring stress and improving the composite's mechanical response [20-23]. In many cases, this allows nanocomposites to achieve comparable or even superior properties using much smaller amounts of fillers [24-26]. Among available nanofillers, multi-walled carbon nanotubes (MWCNTs) have gained significant interest. Their exceptionally high aspect ratio, low density, and outstanding stiffness (with Young's modulus near 1000 GPa) allow for enhanced performance in a wide range of properties, including thermal, electrical, and especially mechanical behavior [27-30]. These advantages make MWCNT-based nanocomposites a key focus in the development of next-generation functional materials [31-33]. Various approaches have been proposed for predicting the mechanical properties of polymer nanocomposites, including experimental techniques, analytical models, and finite element simulations. Several experimental, analytical, and numerical studies have sought to predict the mechanical behavior of polymer nanocomposites[18, 34-36]. For instance, Mortazavian and Fatemi [37] conducted experiments on short fiber-reinforced polymers and reported that tensile strength and elastic modulus are strongly influenced by fiber orientation and material anisotropy. They showed that classical analytical models, such as Tsai–Hill and Halpin–Tsai, can provide reasonable predictions when anisotropic effects are properly accounted for. Similarly, Ghasemi et al. [38] developed an analytical model based on the Takayanagi approach to estimate the tensile modulus of nanocellulose-reinforced composites. Their model explicitly incorporated interphase modulus and filler size as key parameters and demonstrated excellent agreement with experimental measurements, underscoring the critical role of interphase properties in determining overall stiffness. In another example, Bhuiyan et al. [39] employed the finite element analysis (FEA) to predict the tensile modulus of CNT-reinforced polypropylene (PP) composites and systematically investigated the influence of experimentally observed features such as CNT agglomeration, imperfect CNT-polymer interfacial contact, and filler alignment. Their study demonstrated that ignoring these factors led to a substantial overestimation of composite stiffness. When incorporated into the FEA models, these factors brought predictions into close agreement with experimental data. Their findings highlighted that CNT agglomeration and poor interfacial contact reduced the efficiency of reinforcement significantly, while CNT alignment also contributes to variations in the mechanical performance.

While useful, these methods often struggle to account for the complex interactions among multiple factors such as the filler content, aspect ratio, interphase quality, and functionalization. They may also require significant amounts of time and resources to

implement [40-42]. In contrast, machine learning (ML) and artificial neural networks (ANNs) offer a promising data-driven alternative. These models are capable of capturing nonlinear relationships between features, making them particularly useful for predicting the composite behavior based on a range of input parameters. They also help reduce the need for extensive physical testing, and save both time and cost in material development [43, 44]. In recent years, machine learning (ML) and artificial neural networks (ANNs) have been employed in a growing number of studies to predict the physical and mechanical properties of polymer nanocomposites. These models have been used to estimate tensile strength, Young's modulus, thermal conductivity, and other critical properties based on a variety of material descriptors [45, 46]. Their ability to handle nonlinear dependencies and complex feature interactions has made them valuable tools in the field of materials informatics. Champa-Bujaico et al. [47] comprehensively applied machine learning models to predict the mechanical properties of the multiscale nanocomposites based on the poly(3-hydroxybutyrate) (P3HB) reinforced with multi-walled carbon nanotubes (MWCNTs), tungsten disulfide (WS_2), and sepiolite. The results of their studies indicated that the uniform dispersion of these nanofillers significantly enhanced stiffness (by up to 132%), while the improvement in tensile strength was more moderate. Among the models evaluated, the RNN-Levenberg algorithm demonstrated the best performance for predicting Young's modulus, whereas the Random Forest model was the most accurate one for predicting tensile strength. This study demonstrated that machine learning models could predict mechanical properties with high accuracy (R^2 up to 0.92 for test data), as a powerful tool for material design optimization. Rajaee et al. [48] employed the XGBoost algorithm to predict the mechanical properties and fracture behavior of the polypropylene/EPDM nanocomposites reinforced with clay and halloysite nanoparticles. The XGBoost model had excellent accuracy for predicting tensile modulus and strength ($R^2 \approx 0.99$ for test data), while its predictions for more complex variables such as strain at break and essential work of fracture (EWF) were less accurate ($R^2 \approx 0.79$). Their analysis revealed that the nanoparticle content was the most influential parameter, and vulcanization played a critical role in improving mechanical performance. Despite the success of these models, many data-driven studies on polymer nanocomposites still rely primarily on readily accessible descriptors (e.g., matrix properties, filler loading/geometry, and processing conditions) and therefore do not include an explicit interphase modulus parameter, partly due to the limited availability of interphase properties reported in a form suitable for model training [49-51].

This study presents a hybrid framework for predicting the tensile modulus of the thermoplastic polymer nanocomposites reinforced with MWCNTs. A central element of this framework is the interphase modulus, a physically informed parameter derived using an extended version of the Ji model. Unlike traditional features, this one directly captures the effect of the interaction zone between the filler and the matrix. Along with the interphase modulus, other key features used in the models include the polymer matrix modulus, weight fraction of MWCNTs, their diameter and length, and a binary variable indicating functionalization. These features re fed into a set of machine learning models and ANNs, which are trained to predict the tensile modulus accurately. Beyond improving the prediction accuracy, this approach also

highlights which parameters have the most influence, providing materials engineers with a practical tool for optimizing formulation design, tailoring mechanical performance, and accelerating the development of next-generation nanocomposite materials for industrial applications.

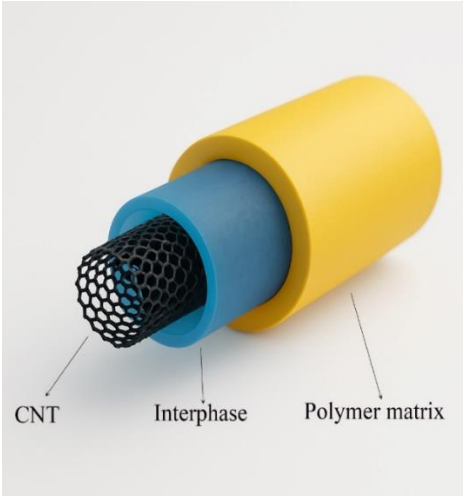

Figure 1. Three-dimensional schematic illustration of a multi-walled carbon nanotube (MWCNT) embedded in a polymer nanocomposite system. The diagram highlights the nanotube core, the surrounding interphase region (shown in blue), and the outer polymer matrix (yellow), which together govern the overall mechanical behavior of the composite.

2. Materials and methods

2.1 Data Description

For this study, a dataset containing 229 data points was compiled from various peer-reviewed publications on polymer nanocomposites. Each data point includes key descriptors such as the Young's modulus of the thermoplastic polymer matrix (E_m), the weight fraction of multi-walled carbon nanotubes (MWCNTs), the diameter and length of the MWCNTs, and a binary variable indicating the functionalization status (0 for pristine, 1 for functionalized). Additionally, the interphase modulus (E_i) was included as a physically informed feature, calculated using an extended version of the Ji model to capture the effect of the interphase region between the matrix and the nanotubes. The representative entries of the compiled experimental dataset are shown in Table 1, while the full descriptive statistics of all features (mean, standard deviation, minimum, and maximum) are provided in the Supplementary Information (Table S1a-b). The complete list of references, from which the dataset was compiled, is available in the References section [52, 53].

Table 1.
Representative sample rows from a dataset compiled in literatures on MWCNT-reinforced thermoplastic nanocomposites, showing the input features (E_m, wt%, E_i, D, L, and functionalization) and the target tensile modulus (E_c). The examples indicate that a given composite system is often reported at multiple wt% levels.

Sample	E_m(GPa)	wt%	E_i(GPa)	D(nm)	L(nm)	Functionalized	E_C(GPa)
PMMA/MWCNT	0.467	1	5.0822	50	5000	0	0.590
		2					0.724
		3					0.854
		5					0.930
		10					0.951
PP/MWCNT	1.38	0.1	5.3017	25	22500	0	1.50
		1					1.55
		3					1.68
		5					1.87
PEN/MWCNT	1.68	0.1	4.4511	20	24000	0	1.76
		0.5					1.87
		0.1	9.041			1	1.84
		0.5					1.98

2.2 Feature Engineering and Preprocessing

To prepare the dataset for machine learning, the combined dataset was first divided into training and testing subsets using a stratified sampling strategy. Specifically, the target variable (tensile modulus, E_c) was discretized into six bins to ensure that both subsets reflected a comparable distribution across the full range of modulus values. An 80:20 split was then applied, resulting in 183 training samples and 46 test samples.

To increase data density along the nanofiller loading axis and facilitate model learning, the training set was augmented using intra-group cubic-spline interpolation. Importantly, interpolation was performed only on the training set after the train/test split, and the test set consisted only of the experimentally reported data that remained intact throughout model development and preprocessing. For augmentation, training samples were grouped according to constant composite descriptors (E_m, D, L, functionalization status, and E_i). Within each group, the relationship between the content of the nanofiller (wt%) and the target modulus (E_c) was interpolated using cubic splines when at least three unique wt% values were available. Intermediate wt% points were generated with a step size of 0.05 wt%, and the corresponding E_c values were computed accordingly. This procedure generated synthetic samples strictly within the original experimental wt% range of each group (i.e., without extrapolation). Using this strategy, the training set was expanded to 4,933 samples.

All numerical input features, including E_m, wt%, E_i, D, and L, were standardized using the StandardScaler function from Scikit-learn to ensure comparable scaling and proportional contribution during model training. The binary functionalization variable (0 or 1) was retained without standardization. To prevent data leakage, the scaler was fitted exclusively on the training subset (on the augmented training data when augmentation was used), and the same fitted scaler was subsequently applied to transform the held-out test set; the test-set statistics were not used at any stage of preprocessing. In addition, for models trained in log space, the target transformation (log1p) was applied only during model fitting on the training targets, and predictions were inverse-transformed (expm1) prior to computing the reported performance metrics.

Because interpolated points are not independent experimental observations, the effect of the spline-based augmentation on generalization was further examined by repeating model training without augmentation under the same split, preprocessing, and hyperparameter settings. The with/without augmentation comparison is provided in the Supplementary Information (Table S2).

2.3 Machine Learning Models and Evaluation

The predictive models implemented in this study included the support vector regression (SVR), random forest regression (RF), gradient boosting regressor (GBR), extreme gradient boosting (XGBoost), k-nearest neighbors (KNN), and artificial neural networks (ANNs). These six algorithms were selected for their ability to model complex nonlinear relationships and have shown promising results in previous studies related to the prediction of material properties.

All model training and validation procedures were carried out in Python using the Scikit-learn and Keras libraries. The model performance was evaluated using three commonly adopted metrics: the coefficient of determination (R^2), mean absolute error (MAE), and root mean squared error (RMSE). These metrics are calculated using Equations (1)– (3).

$$R^2 = 1 - \frac{\sum_{i=1}^{n}(y_i - \hat{y}_i)^2}{\sum_{i=1}^{n}(y_i - \bar{y})^2} \quad (1)$$

$$\mathrm{MAE} = \frac{1}{n}\sum_{i=1}^{n}|y_i - \hat{y}_i| \quad (2)$$

$$\mathrm{RMSE} = \sqrt{\frac{1}{n}\sum_{i=1}^{n}(y_i - \hat{y}_i)^2} \quad (3)$$

Where:

y_i and $\hat{y}_i$ represent the experimental and predicted values for the i-th sample respectively; $\bar{y}$ denotes the mean of the experimental values, and n is the total number of data points.

Hyperparameters for all machine learning models were selected using grid search on the training subset. Candidate hyperparameter combinations were evaluated using 5-fold cross-validation, and the configuration with the best mean cross-validated score was retained. In particular, for the Random Forest model, the search space covered the main parameters of complexity-controlling: n_estimators ∈ {100, 200, 300}, max_depth ∈ {None, 10, 20}, min_samples_split ∈ {2, 5}, and min_samples_leaf ∈ {1, 2}. The complete hyperparameter search spaces for all six models are provided in the Supplementary Information (Table S3), and the final selected settings are summarized in Table S4.

2.4 Calculation of the Interphase Modulus

Ji et al. developed a theoretical model for estimating the Young's modulus of polymer nanocomposites by considering the mechanical contributions of the nanoparticles (p), the interphase region (i), and the polymer matrix (m) [54]. This model has been extended to accommodate various types of nanocomposites and is mathematically expressed as follows [55]:

$$E_r = \left[(1-\alpha) + \frac{\alpha - \beta}{(1-\alpha) + \frac{\alpha(m-1)}{\ln(m)}} + \frac{\beta}{(1-\alpha) + \frac{(\alpha-\beta)(m+1)}{2} + \beta\frac{E_p}{E_m}} \right]^{-1} \quad (4)$$

$$E_r = \frac{E_c}{E_m} \quad (5)$$

$$\beta = \sqrt{Q_f} \quad (6)$$

$$m = \frac{E_i}{E_m} \quad (7)$$

$$\alpha = \sqrt{Q_f + Q_i} \quad (8)$$

A simplified empirical relationship has also been proposed to estimate the effective modulus ratio of polymer nanocomposites based on the combined volume fractions of the nanofiller and interphase regions. This relationship is expressed as [55, 56]:

$$E_r = 1 + 11(Q_f + Q_i)^{1.7} \quad (9)$$

Accordingly, the parameter α can be expressed in terms of E_r as:

$$\alpha = \left(\frac{E_r - 1}{11}\right)^{0.294} \quad (10)$$

To improve the accuracy and generalizability of the original Ji model, Zare and Rhee [55] proposed an extended formulation that integrates interphase properties more explicitly. The resulting expression, which is applicable to a wide range of polymer nanocomposites, is given in Equation (11):

$$E_r = \Bigg[\quad 1-\left(\frac{E_r-1}{11}\right)^{0.294} + \ldots + \frac{\left(\frac{E_r-1}{11}\right)^{0.294} - \sqrt{Q_f}}{1-\left(\frac{E_r-1}{11}\right)^{0.294} + \frac{\left(\left(\frac{E_r-1}{11}\right)^{0.294}\right)\left(\frac{E_i}{E_m}-1\right)}{\ln\left(\frac{E_i}{E_m}-1\right)}} + \frac{\sqrt{Q_f}}{1-\left(\frac{E_r-1}{11}\right)^{0.294} + \frac{1}{2}\left(\left(\frac{E_r-1}{11}\right)^{0.294} - \sqrt{Q_f}\right)\left[\frac{E_i}{E_m}+1\right] + \frac{E_p}{E_m}\sqrt{Q_f}} \Bigg]^{-1} \tag{11}$$

Where E_m, E_i, and E_p denote the Young's modulus of the polymer matrix, the interphase region, and the nanoparticle respectively, and Q_f represents the volume fraction of the nanofiller.

The interphase modulus E_i was calculated using the formulation suggested by Zare and Rhee [55], where it is expressed as a function of the matrix and nanoparticle moduli along with a dimensionless interphase parameter Y, as follows:

$$E_i = E_p - (E_p - E_m)0.5^Y \tag{12}$$

As observed in this relationship, the higher values of Y result in an E_i that approaches the modulus of the nanoparticle (E_p), which in this study corresponds to multi-walled carbon nanotubes (MWCNTs). Conversely, the lower values of Y shift E_i toward the matrix modulus (E_m). In the limiting case, where Y = 0, the interphase region effectively vanishes, and E_i becomes equal to E_m, indicating the absence of a distinct interphase.

To identify the appropriate value of Y, an initial guess is substituted into Equation (12) to compute E_i, which is then used in the Ji-based model (Equation (11)) to predict the effective modulus ratio E_r. The value of Y is updated numerically to minimize the squared mismatch between the predicted and experimental values of E_r, i.e., $\left(E_r^{\text{pred}}(Y) - E_r^{\text{exp}}\right)^2$, and the iteration continues until the mismatch becomes negligibly small (or further updates no longer improve the objective), subject to the physical constraint Y remains non-negative ($Y \geq 0$). In practice, the procedure was initialized with a small Y value in the range [0, 1] (default Y_0 = 0.5), while still allowing convergence to values larger than 1 when required by the experimental data. The complete procedure is schematically illustrated in Figure 2, which outlines the loop of iterative calculations from initial guess to convergence.

It should be noted that the dataset collected from literatures often reports multiple modulus measurements for the same composite system at different nanofiller loadings. Accordingly, in this study, Y (and thus E_i) was estimated once per composite system using a single representative experimental loading level selected from the wt% points reported for that system, and the obtained E_i was then kept constant and assigned to the remaining loading levels of the same system. This strategy reflects the assumption that interphase stiffness is primarily governed by the material pair (polymer/MWCNT and surface state) and

does not vary strongly across the limited wt% range reported for a given system.

In this study, the Young's modulus of MWCNTs (E_p) was set to 1000 GPa as a representative value widely reported for well-graphitized carbon nanotubes. It should be noted that the elastic modulus of MWCNTs reported in the literature can vary depending on the synthesis route, defect density, diameter, and the measurement technique [57-59].

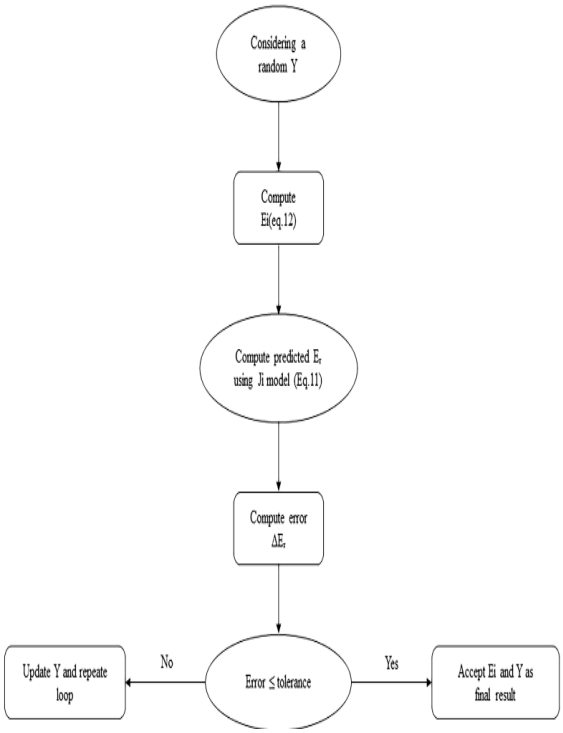

Figure 2. Flowchart illustrating the iterative optimization process used to determine the interphase modulus (E_i). The procedure, implemented in Python using scipy.optimize.minimize, updates the interphase parameter (Y) until the predicted effective modulus (E_r) closely matches the experimental value.

To ensure that our conclusions are not dependent on this assumption, we performed a sensitivity analysis by recalculating the interphase modulus feature using E_p values of 500, 800, 1000, 1200, and 1500 GPa and re-evaluating the predictive performance of the best-performing models (SVR, GBR, and XGBoost) under the same data split and preprocessing pipeline. The test-set metrics showed only minor variations across this E_p range, indicating that the model conclusions are robust to the assumed E_p value. The detailed results are provided in the Supplementary Information (Table S5).[59]

3. Results and Discussion

3.1 Introductory Overview of Results

To evaluate the effectiveness of different machine learning algorithms in predicting the tensile modulus of the polymer nanocomposites reinforced with MWCNTs, a comprehensive series of six models was trained and tested. These included traditional regressors such as the Support Vector Regression (SVR), ensemble-based approaches like Random Forest (RF), Gradient Boosting Regressor (GBR), and XGBoost (XGB), as well as more complex learners such as Artificial Neural Networks (ANN) and instance-based methods like K-Nearest Neighbors (KNN). The goal was to compare these models not only through classical evaluation metrics such as R^2, MAE, and RMSE, but also in terms of their generalization ability, cross-validation stability, and overall interpretability. The model performance was assessed using a consistently prepared dataset that incorporated careful preprocessing steps, including the log-transformation of the target variable and data augmentation via cubic spline interpolation. By systematically tuning hyperparameters and applying cross-validation strategies, the study aimed to identify the most reliable and accurate predictive model. The following sections provide a detailed breakdown of model performances, error trends, and key insights into how the model structure influences the predictive behavior.

3.2 Overall Comparison of Model Performances

A broad performance overview revealed that most machine learning models demonstrated satisfactory accuracy in predicting the tensile modulus, with several models achieving test-set R^2 scores above 0.95. Among these, ensemble-based models, particularly GBR and XGB, consistently yielded the best results, striking an effective balance between accuracy and generalization. These methods achieved low MAE and RMSE values while avoiding overfitting, a testament to their robustness across varying data splits. Artificial Neural Networks (ANNs), while inherently more complex, performed comparably well when carefully tuned. The sensitivity of ANNs to hyperparameters was evident, yet when properly configured, their predictive strength rivaled the best ensemble models. Meanwhile, simpler models such as KNN, despite their reduced flexibility, still managed to produce solid results, largely due to the informative nature of the engineered feature set and the preprocessing pipeline. These findings underscore that, although advanced models offer higher accuracy and adaptability, simpler approaches can still be competitive in well-structured settings. The implication is that the thoughtful data preparation can significantly enhance the performance of even the most basic algorithms.

3.3 Performance Comparison Across Models

The numerical results of all six models are summarized in Table 2. The Gradient Boosting Regressor (GBR) emerged as the top-performing model, achieving a test R^2 of 0.9868 with a remarkably low MAE of 0.0765 and RMSE of 0.1381. This demonstrates that GBR has effectively captured the nonlinear structure of the data and generalized well across unseen samples. XGBoost and SVR also delivered strong performances, with test R^2 values above 0.98, highlighting the strength of boosting algorithms and kernel-based methods in modeling complex relationships. Artificial Neural Networks (ANNs) achieved competitive results (test R^2 = 0.9703), reflecting their ability to capture nonlinear dependencies and interactions between features. However, their sensitivity to hyperparameter settings was evident, and their performance remained more dependent on how these settings were tuned, particularly as network architectures became deeper or more complex.

Random Forest (RF) displayed a near-perfect fit on the training data (R^2 = 0.9999) but exhibited a noticeable reduction in the test performance (R^2 = 0.9527), suggesting mild overfitting. Although this drop is not critical, it underscores the importance of the careful model validation when applying RF to heterogeneous datasets. The K-Nearest Neighbors (KNN) algorithm, while conceptually simple, performed better than expected, achieving a test R^2 of 0.9795 and demonstrating solid effectiveness on datasets with localized patterns.

Taken together, these results illustrate a clear trade-off between the model complexity and performance stability. Ensemble methods and ANNs offered superior predictive accuracy but required more careful tuning and training resources, whereas simpler algorithms such as KNN remained surprisingly competitive, due to the strength of the engineered features and preprocessing pipeline.

Table 2.
Evaluation results (R^2, MAE, RMSE) of the machine learning models on the train and test datasets. Overall, GBR achieves the highest test-set accuracy (R^2 = 0.9868; RMSE = 0.1381 GPa) with a small train–test gap, whereas RF shows the largest generalization gap (R^2: 0.9999 train vs. 0.9527 test), consistent with higher variance/overfitting tendencies.

	R^2		MAE		RMSE	
Model	Train	Test	Train	Test	Train	Test
SVR	0.9911	0.9826	0.0881	0.1112	0.1486	0.1584
GBR	0.9992	0.9868	0.0267	0.0765	0.0439	0.1381
RF	0.9999	0.9527	0.0016	0.1292	0.0150	0.2612
XGBoost	0.9992	0.9837	0.0270	0.0889	0.0436	0.1534
KNN	0.9996	0.9795	0.0015	0.1061	0.0307	0.1719
ANN	0.9667	0.9703	0.1364	0.1131	0.2872	0.2067

3.3.1. Comparison with an analytical baseline (Halpin–Tsai model)

In addition to the model-to-model comparison in Table 2, an analytical micromechanics baseline was introduced to provide a reference point against the classical composite theory. Specifically, the Halpin–Tsai formulation was used to estimate the tensile modulus of the MWCNT-reinforced nanocomposites from the matrix modulus and filler content. For each experimental sample, the nanotube volume fraction V_f was computed from the reported weight fraction and densities, ensuring consistency across material systems. The Halpin–Tsai modulus was then calculated as:

$$E_{\mathrm{HT}} = E_m \frac{1+\xi\eta V_f}{1-\eta V_f} \tag{13}$$

$$\eta = \frac{\left(\frac{E_f}{E_m}\right)-1}{\left(\frac{E_f}{E_m}\right)+\xi} \tag{14}$$

$$\xi = 2\frac{L}{D} \tag{15}$$

where E_m is the matrix modulus, E_f is the nanotube modulus, and ξ is the geometry parameter. In this baseline, ξ was set using the nanotube aspect ratio to reflect the high-aspect-ratio nature of MWCNTs.

It should be noted that Halpin–Tsai does not explicitly capture the key nanoscale effects such as the interphase mechanics, dispersion/agglomeration, imperfect load transfer, and processing-induced variability; therefore, it is used here strictly as a simplified baseline rather than a calibrated predictive model. The baseline predictions were evaluated on the same experimental train/test split used throughout the manuscript (i.e., without using spline-generated augmented samples for evaluation). The resulting performance metrics are summarized in Table 3, and a brief comparison confirms that the best-performing ML models substantially outperform the analytical baseline on the independent test set, highlighting the benefit of data-driven learning combined with physically meaningful descriptors.

Table 3.
Test-set performance comparison between the Halpin–Tsai analytical baseline and the top ML models (evaluated on the experimental-only test set). The analytical baseline exhibits substantially lower agreement with experiments (R^2 = 0.432; RMSE = 0.739 GPa), while ML models markedly improve the predictive accuracy, highlighting the benefit of data-driven learning for the heterogeneous literature dataset.

Model	R^2 (Test)	MAE (Test) [GPa]	RMSE (Test) [GPa]
Halpin–Tsai (baseline)	0.432	0.341	0.739
GBR	0.9868	0.0765	0.1381
XGBoost	0.9837	0.0889	0.1534
SVR	0.9826	0.1112	0.1584

The Halpin–Tsai analytical baseline exhibits limited agreement with the experimental data, yielding R^2 = 0.432, MAE = 0.341 GPa, and RMSE = 0.739 GPa on the experimental-only evaluation set. This outcome is expected because Halpin–Tsai is a simplified micromechanics formulation that does not explicitly capture nanoscale effects governing CNT nanocomposites, including interphase mechanics, dispersion/agglomeration, imperfect load transfer, and processing-induced variability. In contrast, the top performing machine learning models provide substantially improved predictive performance on the same independent test set (e.g., $R^2 \approx$ 0.98 with RMSE ≈ 0.14–0.16 GPa), highlighting the added value of the data-driven framework and the inclusion of physically informed descriptors such as the interphase modulus.

3.4 Scatter Plot Analysis

To further understand the predictive behavior of each model, scatter plots of predicted versus actual tensile modulus values were examined for both the training and test sets. These plots provide visual insight into the accuracy, generalization capability, and any systematic biases or variance present in the predictions. Ideally, a well-performing model should produce data points closely aligned along the identity line (y = x), indicating consistent accuracy across the entire range of values.

Among the evaluated models, the Support Vector Regression (SVR) exhibited a balanced and robust performance. On the training set, it achieved an R^2 of 0.9911 and RMSE of 0.1486 GPa, while maintaining a high R^2 of 0.9826 with a low RMSE of 0.1584 GPa on the test set. These results suggest that SVR effectively captured the underlying data patterns without overfitting. The scatter plots further confirm this behavior, showing a tight clustering of predicted values around the ideal diagonal line for both training and test datasets, reflecting excellent generalization. Notably, the SVR's ability to deliver this level of performance, despite a limited number of input features, highlights its strength in modeling nonlinear relationships when properly tuned. In addition, the small difference between training and test errors indicates high stability and reliable predictive capacity across the dataset.

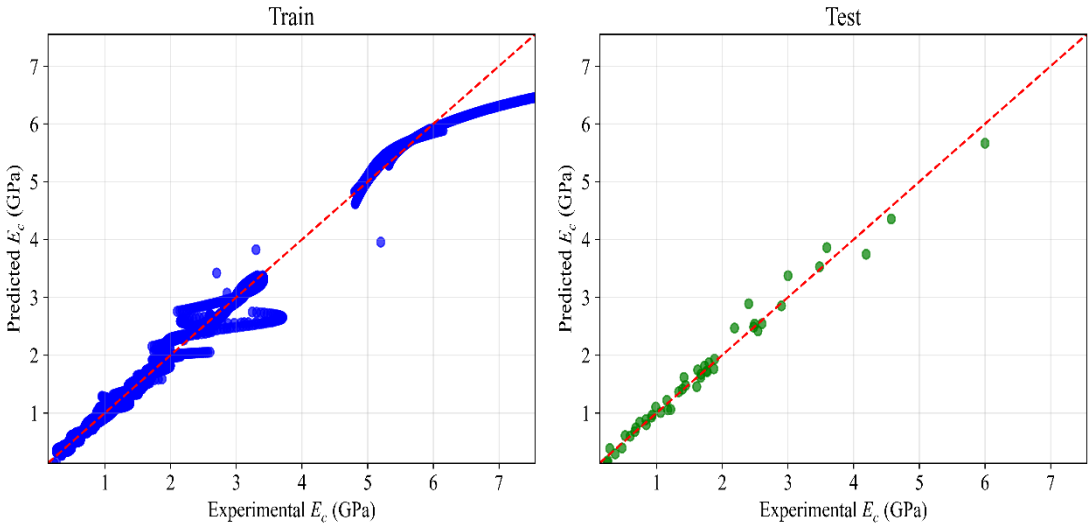

Figure 3. Scatter plot of predicted versus experimental tensile modulus values using the Support Vector Regression (SVR) model

Among all the models tested, the Gradient Boosting Regressor (GBR) achieved the highest predictive accuracy on the test set, with an R^2 of 0.9868 and an RMSE of 0.1381 GPa, indicating excellent agreement between predicted and true values. On the training set, the model yielded near-perfect metrics (R^2 = 0.9992, RMSE = 0.0439 GPa), demonstrating its strong capacity to learn the data structure. Importantly, the relatively small gap between training and test results suggests that overfitting was effectively minimized, aided by careful hyperparameter tuning and regularization. The corresponding scatter plots display a dense clustering of predictions along the ideal y = x line for both subsets, illustrating GBR's consistency and generalization. Overall, these results highlight GBR's ability to capture complex feature interactions and non-linear patterns, making it a particularly effective approach for predicting material properties from structured datasets.

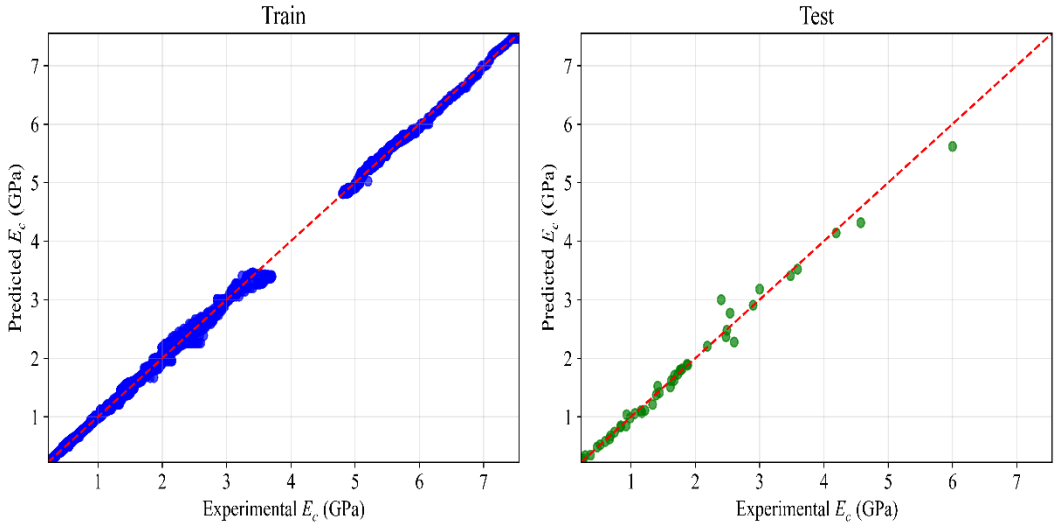

Figure 4. Scatter plot of predicted versus experimental tensile modulus values using the Gradient Boosting Regressor (GBR) model

The Random Forest (RF) achieved near-perfect training performance (R^2_train ≈ 1.00) while yielding a lower, though still high, test performance (R^2_test = 0.9527), indicating a degree of overfitting. Such a train–test generalization gap is consistent with the high-variance behavior of tree ensembles, particularly when trees are allowed to grow relatively deep and leaf nodes can contain very few samples, which increases model flexibility and can capture study-specific noise in heterogeneous literature-derived datasets. Moreover, the partial redundancy among tabular descriptors and the redundancy introduced by spline-based augmentation along the wt% axis can further facilitate the memorization of training patterns by flexible ensembles. Importantly, RF hyperparameters were selected using the 5-fold cross-validated grid search; however, a residual generalization gap persisted, which is expected for variance-dominated learners on multi-source experimental datasets. Therefore, RF results are reported as high-performing but interpreted with appropriate caution alongside more stable learners such as SVR.

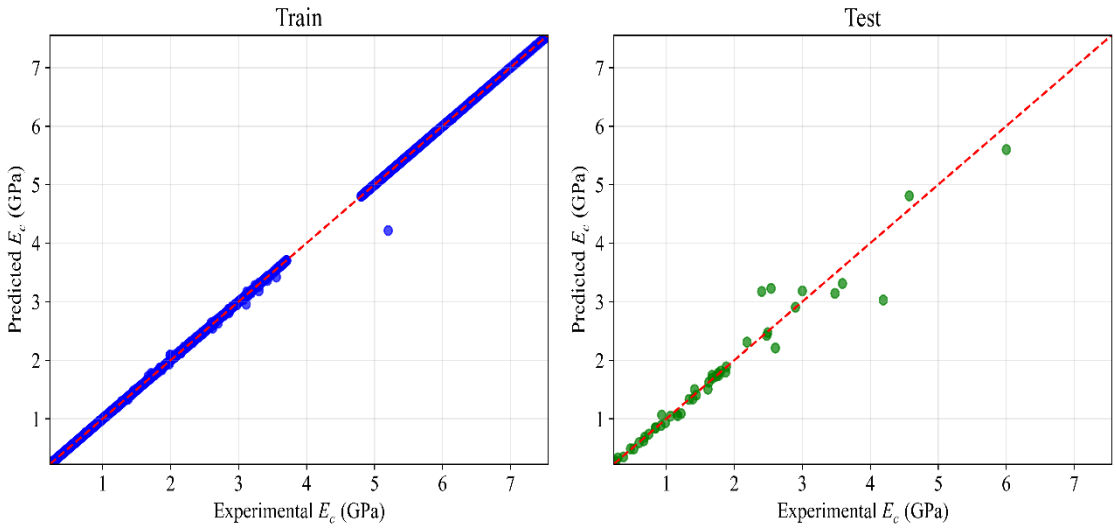

Figure 5. Scatter plot of predicted versus experimental tensile modulus values using the Random Forest (RF) model

XGBoost (Extreme Gradient Boosting) demonstrated one of the most accurate and consistent performances among all models evaluated. On the training set, it achieved an excellent R^2 of 0.9992 with a very low RMSE of 0.0433 GPa, indicating that it learned the underlying data patterns nearly perfectly. Importantly, its performance on the test set remained highly competitive, with an R^2 of 0.9832 and RMSE of 0.1556 GPa. The narrow performance gap between training and test results suggests that XGBoost was able to generalize effectively without overfitting. The corresponding scatter plots show a tight clustering of predictions along the ideal diagonal for both training and test sets, further reinforcing the model's robustness. This behavior underscores XGBoost's capability to capture complex, nonlinear interactions with a relatively modest number of input features and minimal preprocessing. Moreover, the model exhibited strong stability across different runs and hyperparameter configurations, making it a particularly reliable choice for predictive tasks in materials informatics. Overall, XGBoost stands out for its combination of high predictive accuracy, excellent generalization, and computational efficiency,

highlighting its potential as a robust tool for materials design and property prediction.

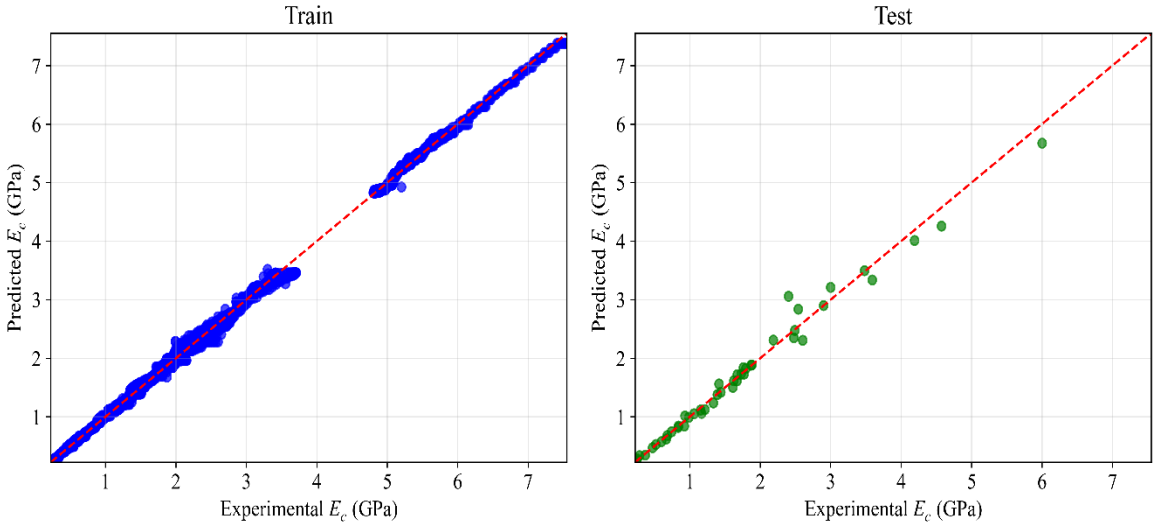

Figure 6. Scatter plot of predicted versus experimental tensile modulus values using the XGBoost model.

Despite its conceptual simplicity, the K-Nearest Neighbors (KNN) algorithm delivered unexpectedly competitive results in this study. Using an optimal configuration of three neighbors, the model achieved a test R^2 of 0.9795 and an RMSE of 0.1719 GPa, placing its performance close to that of more sophisticated algorithms such as SVR and XGBoost. On the training set, KNN reported a near-perfect R^2 of 0.9996; while this exceptionally high value reflects the model's ability to replicate known data, it should be interpreted with caution due to KNN's inherent sensitivity to the training samples. The scatter plots for both training and test sets revealed a dense clustering of points around the ideal y = x line, particularly in the mid-range of the target variable. However, slightly greater dispersion was observed at the extremes, which is a typical limitation of instance-based approaches like KNN. Overall, the model's strong performance can be attributed more to the quality of the input features and preprocessing pipeline than to the intrinsic learning capabilities of KNN itself. These findings illustrate that, for regression tasks involving well-structured and relatively noise-free datasets, even simple non-parametric, memory-based methods such as KNN can achieve robust and reliable predictive accuracy.

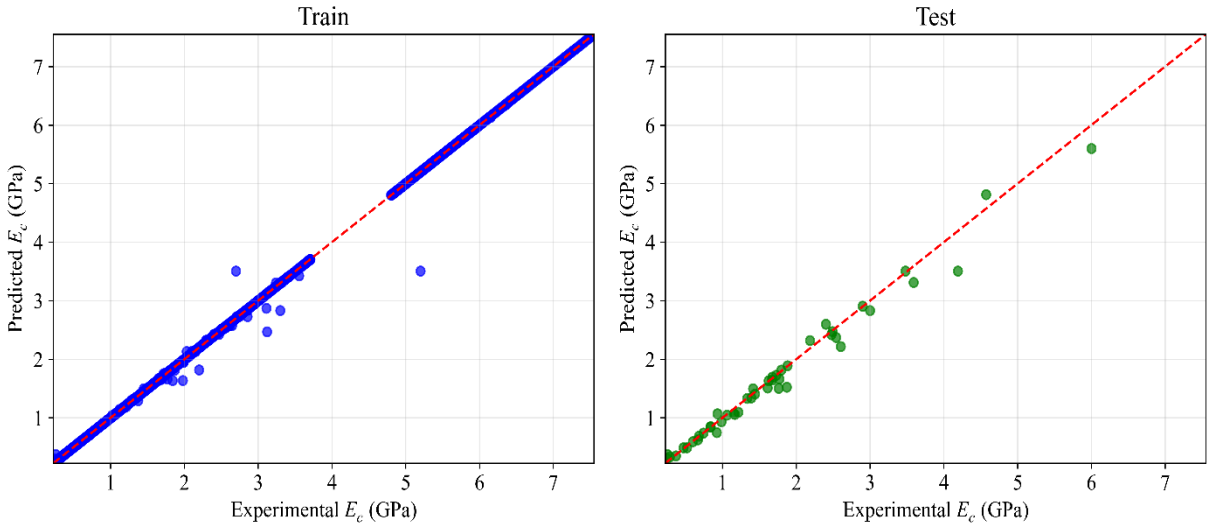

Figure 7. Scatter plot of predicted versus experimental tensile modulus values using the k-Nearest Neighbors (KNN) model

Among all artificial neural network (ANN) configurations evaluated in this study, the best-performing architecture consisted of two hidden layers with 16 units each, ReLU activation functions, batch normalization, a dropout rate of 0.1, and the Adam optimizer with a learning rate of 0.001. Using a batch size of 16, this model achieved an R^2 of 0.9668 on the training set and 0.9703 on the test set, with corresponding MAE values of 0.1364 GPa and 0.1132 GPa and RMSE values of 0.2872 GPa and 0.2067 GPa respectively.

Although the overall trend of predictions follows the ideal diagonal line, the training scatter plot exhibits noticeable dispersion, particularly in the mid to high modulus range, reflecting the sensitivity of ANNs to localized variations in the non-uniformly interpolated training data. In contrast, the test scatter plot, which contains only real experimental samples, appears more compact, indicating that the model generalizes reasonably well despite the variability observed in training.

Additional ANN architectures were evaluated, and their detailed performance metrics are summarized in the Supplementary Information (Table S6). Several of these configurations demonstrated comparable accuracy; however, their prediction errors were less uniform across the modulus range, particularly in regions with limited experimental coverage. These comparisons confirm that the selected two-layer, 16-unit architecture offers the most reliable balance between accuracy, robustness, and model complexity.

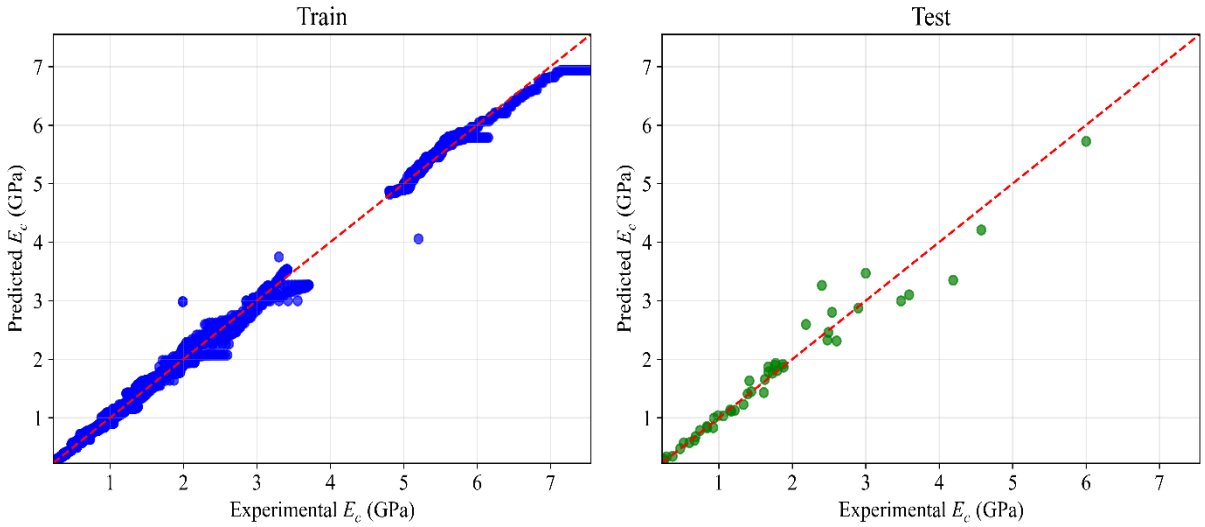

Figure 8. Scatter plot of predicted versus experimental tensile modulus values using the Artificial Neural Network (ANN) model.

3.5 Cross-validation and Generalization

To further assess the generalization capabilities of the developed models, a 5-fold cross-validation (CV) procedure was performed exclusively on the augmented training dataset, ensuring that the test set remained intact for unbiased evaluation. Three models, SVR, XGBoost, and the best-performing ANN architecture, were selected for this evaluation based on their earlier results.

Specifically, a single (non-repeated) 5-fold KFold scheme (n_splits = 5), with shuffling enabled and a fixed random seed (random_state = 42), was adopted to ensure reproducibility. In each fold, the model was trained on four folds and evaluated on the held-out fold, and the reported CV metrics represent the mean performance across the five folds. The fold-level stratification was not applied in the CV procedure; however, the initial 80:20 train–test split was stratified by discretizing the target variable (E_c) into six quantile-based bins to preserve a comparable modulus distribution across the training and test subsets. For models trained in log space, predictions were back-transformed prior to computing the reported CV metrics.

The SVR model demonstrated exceptional consistency and stability across folds, achieving a mean R^2 of 0.9904, MAE of 0.0895, and RMSE of 0.1538, indicating robust generalization and minimal variance. XGBoost further reinforced its strong performance with a mean R^2 of 0.9988, MAE of 0.0300, and RMSE of 0.0529, confirming its capability to capture non-linear patterns with outstanding accuracy and stability.

In contrast, the ANN model showed noticeably lower performance, with a mean R^2 of 0.7486, MAE of 0.4136, and RMSE of 0.7815, during cross-validation. This drop compared to that of its single train–test split performance ($R^2 \approx 0.970$) indicates higher sensitivity to data partitioning. Plausible explanations include variability in the fold-wise sample composition for a heterogeneous literature-derived dataset, the stochastic nature of neural-network training (e.g., sensitivity to initialization and convergence to different local minima across folds), and an architecture that performs strongly on a single split but is less robust under fold-to-fold distribution shifts.

Overall, the cross-validation analysis indicates that SVR and XGBoost provide consistently

strong and stable generalization under fold-based evaluation, whereas ANN may require additional regularization, architecture refinement, or larger datasets to achieve comparable robustness. Detailed fold-by-fold CV results for these models are provided in the Supplementary Information (Table S7).

To further complement the fold-based CV analysis and directly assess the potential overfitting behavior as a function of data availability, learning-curve diagnostics were additionally generated for representative models. Specifically, the Random Forest (as a high-capacity model prone to variance) and SVR (as a stable top-performing baseline) were evaluated by plotting the training RMSE and 5-fold CV RMSE against progressively increasing training set sizes, using both the non-augmented experimental training subset and the augmented training subset. These curves, reported in the Supplementary Information (Figs. S3–S4), show that the cross-validated error decreases and gradually approaches a plateau as more data become available, indicating that the models improve primarily through increased data coverage rather than memorization. Moreover, SVR exhibits a consistently small train–CV gap, whereas the Random Forest retains a modest gap that is consistent with mild variance-driven overfitting under heterogeneous literature-derived data. Importantly, all preprocessing steps (including feature scaling) were performed in a leakage-safe manner within each CV split using pipeline-based fitting, ensuring that the reported learning curves reflect unbiased generalization trends.

3.6 Discussion on Interphase Modulus Feature

In polymer nanocomposites reinforced with MWCNTs, the interphase region plays a critical role in facilitating stress transfer between the polymer matrix and the nanofillers. Consequently, the inclusion of the interphase modulus (E_i) as an input feature was expected to substantially enhance the predictive capability of the models. To rigorously assess its importance, both drop-column analysis and additional architecture exploration were performed. In the drop-column analysis, three core models, SVR, XGBoost, and the best-performing ANN, were retrained after removing E_i from the feature set. In all cases, the model performance deteriorated noticeably. For SVR, the test R^2 dropped from 0.9826 to 0.9079, and RMSE increased from 0.1584 to 0.3644 GPa. Similarly, XGBoost saw a reduction in test R^2 from 0.9837 to 0.9804, and the ANN performance declined even more severely, with the test R^2 decreasing from 0.9703 to 0.8061. This consistent drop confirms that E_i carries essential information directly related to the mechanical behavior of the composites.

Additionally, a new exhaustive grid search was conducted to find the best ANN architectures in the absence of E_i. Despite this effort, none of the resulting models could match the performance levels achieved when E_i was included. The top-performing ANN without E_i attained a test R^2 of 0.9165, still significantly below the best ANN result with E_i present ($R^2 = 0.9714$).

These findings underscore that while advanced machine learning architectures can partially compensate for missing information, they cannot fully recover the predictive power that a physically meaningful feature like E_i provides. The presence of E_i directly captures the effects of the interaction zone between the filler and the matrix, which is otherwise difficult for data-driven algorithms to infer from secondary descriptors alone. In summary, this analysis demonstrates the critical importance of including physically-informed features such as the interphase modulus when predicting the mechanical properties of

polymer nanocomposites. Not only does E_i improve the overall model accuracy, but it also enables simpler and more stable architectures to generalize effectively, thereby reducing the risk of overfitting or high-variance behavior in the modeling process.

Table 4.
Performance of SVR, XGBoost, and ANN after removing the interphase modulus (E_i) feature. Removing E_i leads to a pronounced degradation for SVR (test R^2 drops to 0.9079) and ANN (test R^2 drops to 0.8061), confirming the strong predictive contribution of E_i, while XGBoost remains comparatively robust (test R^2 = 0.9804).

	R^2		MAE		RMSE	
Model	Train	Test	Train	Test	Train	Test
XGBoost	0.9990	0.9804	0.0312	0.1027	0.0505	0.1682
SVR	0.9790	0.9079	0.1273	0.2030	0.2281	0.3644
ANN	0.8296	0.8061	0.3293	0.3058	0.6505	0.5286

In addition, model interpretability was investigated using a SHAP summary (beeswarm) plot computed for the trained XGBoost model (Figure 9). In this representation, features are ordered by their mean absolute SHAP values (global importance), while the sign of SHAP values indicates whether a feature increases or decreases the model output relative to the baseline. As shown in Figure 9, E_m exhibits the broadest SHAP distribution, indicating the strongest overall contribution to the model predictions, followed by wt% and E_i, whereas L, Func, and D display comparatively smaller contributions clustered near zero. Directionality can be inferred from the color–position pattern: the higher values of E_m (red points) predominantly correspond to positive SHAP values, indicating that stiffer matrices tend to increase the predicted tensile modulus. A similar trend is observed for E_i, where higher interphase modulus values generally shift predictions upward. For wt%, higher loadings tend to contribute positively overall, although the presence of both positive and negative SHAP values suggests non-linear effects and interactions with other descriptors. Because the XGBoost model was trained on a log-transformed target, SHAP values quantify contributions in the model output space; nevertheless, the relative ranking and directional trends remain informative for the physical interpretation.

Together, the drop-column and SHAP analyses reinforce the critical role of the interphase modulus in predicting the tensile behavior of polymer nanocomposites. Excluding this feature not only reduces model accuracy but also undermines the physical interpretation of the system. Therefore, modeling approaches the explicitly incorporate E_i, derived from physically motivated analytical formulations, tend to exhibit higher reliability and stronger generalization performance.

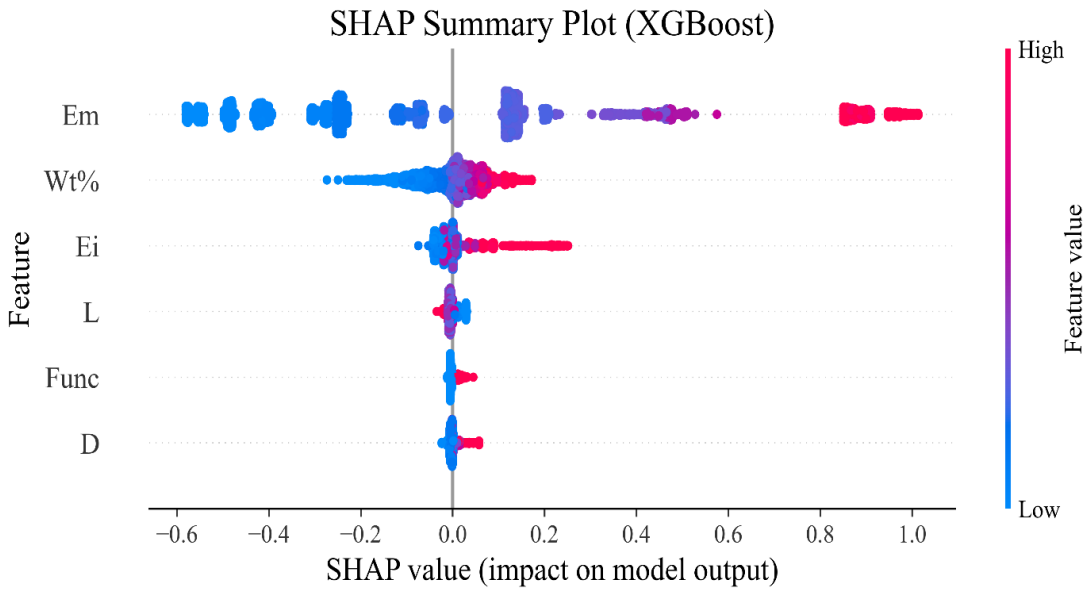

Figure 9. SHAP summary plot for the XGBoost model. Features are ranked by the mean absolute SHAP value (global importance). Points represent samples and are colored by the feature value (blue: low, red: high). The x-axis shows signed SHAP values (impact on the model output): positive values increase the prediction relative to the baseline, while negative values decrease it.

3.7 Best Model Architecture

Among all machine learning models evaluated in this study, the Artificial Neural Network (ANN) demonstrated strong capability in modeling the non-linear relationships between input features and the target tensile modulus. Although tree-based ensemble methods such as XGBoost and Gradient Boosting achieved slightly superior overall accuracy, the ANN remained competitive and offered valuable flexibility in the architectural customization.

Following an extensive grid search across hyperparameters, the best-performing ANN architecture consisted of two hidden layers, each containing 16 neurons, employing ReLU activation functions. To promote training stability and prevent overfitting, Batch Normalization and a Dropout rate of 0.1 were applied after each hidden layer. The network was optimized using the Adam optimizer with a learning rate of 0.001 and trained with a batch size of 16. This configuration yielded a training R^2 of 0.9668 and a test R^2 of 0.9703, with a test MAE of 0.1132 GPa and RMSE of 0.2068 GPa, indicating a robust fit and strong generalization performance. The narrow gap between training and test metrics confirms that the model successfully avoided overfitting while maintaining high predictive accuracy.

The use of ReLU activations ensured efficient gradient propagation without introducing unnecessary complexity, while Batch Normalization accelerated convergence, and Dropout provided regularization. The relatively shallow network depth also contributed to reduced computational costs and faster training, making this architecture practical for use in material design workflows. Overall, this ANN architecture achieved an effective balance between complexity, stability, and predictive performance, establishing it as a reliable model for predicting tensile modulus in polymer nanocomposites.

3.8 Error Analysis and Limitations

Despite the generally high accuracy achieved across all models, the residual analysis and

scatter plots revealed specific regions where the prediction performance declined. Simpler algorithms such as KNN performed remarkably well overall (Test R^2 = 0.9795), with the dense clustering of predictions along the ideal line. However, minor deviations were observed for several samples at higher modulus values, consistent with KNN's sensitivity to the local data density and its reliance on neighboring instances for prediction. Advanced models also exhibited characteristic behaviors: ANN, despite achieving strong performance on the test set ($R^2 \approx 0.97$), showed noticeable variability under 5-fold cross-validation (mean $R^2 \approx 0.74$), indicating sensitivity to data partitioning and architectural configuration. In contrast, SVR maintained stable performance across folds, reflecting its robustness and lower sensitivity to dataset heterogeneity.

To further diagnose whether the observed deviations at higher modulus values reflect the systematic model bias, residual-versus-predicted plots were examined for the two strongest ensemble models (GBR and XGBoost). The residual patterns remain broadly centered around zero with no clear monotonic trend, suggesting the absence of a pronounced global bias. However, a modest increase in residual dispersion is observed at larger predicted E_c values, indicating mild heteroscedasticity. This behavior is consistent with the lower data density and higher heterogeneity of high-modulus samples within a literature-compiled dataset. Residual diagnostics were generated using only experimental (non-augmented) samples for both the training subset and the independent test set, and the corresponding plots are provided in the Supplementary Information (Figure S2).

A major source of prediction error stems from the intrinsic variability of the experimental data collected from multiple literature sources, where differences in material systems, processing routes, dispersion quality, polymer grade, specimen preparation, and measurement protocols introduce unavoidable inter-study heterogeneity. This variability acts as an additional noise source and may limit strict transferability to a single laboratory or a fixed manufacturing route, even when overall predictive trends are captured accurately. Therefore, the reported test performance should be interpreted primarily as generalization across the pooled literature domain rather than a guaranteed accuracy for any specific processing condition without additional calibration. Although stratified train–test splitting and feature standardization were applied to reduce distribution imbalance and scaling effects, perfect consistency cannot be expected in such a heterogeneous compilation. Furthermore, correlations among certain descriptors (e.g., nanotube diameter and length) may introduce partial redundancy, which can contribute to mild overfitting in some models, such as Random Forest, where near-perfect training accuracy does not fully translate to the test set.

Another limitation is that the framework relies on engineered tabular descriptors, which, although physically meaningful, cannot fully capture microstructural factors such as dispersion state, agglomeration, interfacial adhesion quality, and processing-induced morphology factors that strongly influence mechanical behavior but difficult to quantify consistently from published reports. Future work could strengthen the model transferability by incorporating richer metadata (e.g., processing conditions, characterization indicators of dispersion, and test protocol details) when available, or by developing domain-specific models that are tailored to particular polymer families or processing routes. An additional limitation

relates to the interpolation-based data augmentation strategy. The cubic-spline augmentation increases data density along the wt% axis, but the generated samples are not independent experimental observations and, if misused, could lead to optimistic performance estimates. In this work, this risk was reduced by applying interpolation only to the training set after the train/test split, while the test set contained only experimentally reported data. Moreover, the effect of augmentation on generalization was explicitly examined by re-training the best-performing models without augmentation using the same split, preprocessing, and hyperparameters; the comparison (with vs. without augmentation) is reported in the Supplementary Information (Table S2). Overall, the ablation results support that the adopted augmentation strategy does not artificially inflate performance and can improve predictive generalization for the selected models.

3.9 Summary of Findings

The comparative analysis of six machine learning models revealed distinct performance patterns in predicting the tensile modulus of MWCNT-reinforced polymer nanocomposites. Ensemble-based models, particularly XGBoost and Gradient Boosting Regressor, consistently achieved the highest predictive accuracy, combining strong generalization with robustness to data variability. SVR also performed competitively, benefiting from its kernel-based capacity to model non-linear relationships.

Among these, ANN demonstrated acceptable accuracy on the test set but exhibited greater sensitivity during cross-validation, reflecting its dependence on training configuration and data distribution. Importantly, the inclusion of the interphase modulus (E_i) significantly enhanced the model performance across all algorithms. The drop-column analysis confirmed that excluding E_i led to performance degradation, especially for ANN and SVR, while XGBoost showed a smaller drop, highlighting its resilience. The SHAP analysis further validated E_i as one of the top influential features, showing that higher E_i values strongly contributed to increased tensile modulus predictions, consistent with the physical understanding of interphase reinforcement.The scatter plot analysis supported these findings by illustrating tight clustering around the ideal prediction line for high-performing models, particularly tree-based ensembles. Overall, this phase of the study established a robust and reproducible modeling framework, demonstrated the critical role of feature engineering, particularly the interphase modulus, and identified XGBoost and SVR as powerful and reliable tools for predictive modeling in nanocomposite material design.

4. Conclusions

In this study, a comprehensive framework was developed for predicting the tensile modulus of thermoplastic polymer nanocomposites reinforced with multi-walled carbon nanotubes (MWCNTs) using machine learning (ML) algorithms and artificial neural networks (ANNs). The dataset combined the features such as the polymer matrix modulus, MWCNT weight fraction, dimensions, functionalization status, and interphase modulus (E_i), which was derived obtained using an extended Ji model. Among the six models evaluated, the ensemble-based algorithms, particularly XGBoost and Gradient Boosting Regressor (GBR), achieved the highest predictive accuracy, with the test R^2 values exceeding 0.98. SVR and ANN models also delivered competitive results, especially when tuned carefully. The inclusion of E_i as an input feature was found to significantly improve the prediction performance across all models, as

demonstrated by both the drop-column analysis and SHAP interpretability assessments. Cross-validation experiments confirmed the generalization capabilities of the top-performing models, although ANN exhibited greater sensitivity to training data partitioning and configuration choices. The error analysis further highlighted model-specific limitations, especially in regions with higher tensile modulus values or underrepresented feature combinations. Overall, this work demonstrates the effectiveness of combining domain-specific feature engineering with modern ML methods to improve the predictive accuracy and extract interpretable insights into the structure-property relationships of polymer nanocomposites. Future research should aim to expand the dataset with higher-quality experimental records, incorporate additional features capturing microstructural details (e.g., dispersion uniformity, interfacial bonding), and explore uncertainty-aware modeling approaches to further enhance reliability and applicability in material design optimization.

Data and Code Availability

The dataset has been compiled from peer-reviewed literature sources, and key modeling details are provided in the manuscript and Supplementary Information. The Python scripts used for preprocessing, Ei computation, augmentation, and model training/evaluation are available from the corresponding author upon the reasonable request for academic and reproducibility purposes.

References

[1] Chanda M, Roy SK (2008) Industrial polymers, specialty polymers, and their applications. CRC press, NewYork.

[2] Tonelli AE, Srinivasarao M (2001) Polymers from the inside out: an introduction to macromolecules. MRS Bull 4:1024. https://doi.org/10.1557/mrs2001.280.

[3] Sharifzadeh E, Rahimi M, Azimi N, Abolhasani M (2024) Thermal management of photovoltaic panels using phase change materials and hierarchical ZnO/expanded graphite nanofillers. Energy 306:132324. https://doi.org/10.1016/j.energy.2024.132324.

[4] Sharifzadeh E, Cheraghi K (2021) Temperature-affected mechanical properties of polymer nanocomposites from glassy-state to glass transition temperature. Mech Mater 160:103990. https://doi.org/10.1016/j.mechmat.2021.103990.

[5] Sharifzadeh E, Mohammadi R (2021) Temperature-/Frequency-dependent complex viscosity and tensile modulus of polymer nanocomposites from the glassy state to the melting point. Polym Sci Eng 61(10):2600–15. https://doi.org/10.1002/pen.25786.

[6] Sharifzadeh E, Ghasemi I, Karrabi M, Azizi H (2014) A new approach in modeling of mechanical properties of binary phase polymeric blends. Iran Polym J 23(7):525–30. http://doi.org/10.1007/s13726-014-0247-6.

[7] Sharifzadeh E (2021) Evaluating the dependency of polymer/particle interphase thickness to the nanoparticles content, aggregation/agglomeration factor and type of the exerted driving force. Iran Polym J 30(10):1063–72. http://doi.org/10.1007/s13726-021-00956-3.

[8] Sharifzadeh E, Amiri Y (2020) The effects of the arrangement of Janus nanoparticles on the tensile strength of blend-based polymer nanocomposites. Polym Compos 41(9):3585–93. https://doi.org/10.1002/pc.25645.

[9] Groover MP (2010) Fundamentals of modern manufacturing: materials,

processes, and systems. John Wiley & Sons, Danvers.

[10] Sharifzadeh E, Ghasemi I, Karrabi M, Azizi H (2014) A new approach in modeling of mechanical properties of nanocomposites: effect of interface region and random orientation. Iran Polym J 23(11):835–45. http://doi.org/10.1007/s13726-014-0276-1.

[11] Sharifzadeh E, Karami M, Ader F (2023) Formation of nanoparticle aggregates and agglomerates in polymer nanocomposites and their distinct impacts on the mechanical properties. Polym Eng Sci 63(4):1303–13. https://doi.org/10.1002/pen.26284.

[12] Sharifzadeh E (2019) Modeling of the Mechanical Properties of Blend Based Polymer Nanocomposites Considering the Effects of Janus Nanoparticles on Polymer/Polymer Interface. Chin J Polym Sci 37(2):164–77. http://doi.org/10.1007/s10118-019-2178-3.

[13] Mohammadi R, Sharifzadeh E, Azimi N (2024) Temperature-dependent storage modulus of polymer nanocomposites, blends and blend-based nanocomposites based on percolation and De Gennes's self-similar carpet theories. Iran Polym J 33(7):877–90. https://doi.org/10.1007/s13726-024-01300-1.

[14] Shameem MM, Sasikanth S, Annamalai R, Raman RG (2021) A brief review on polymer nanocomposites and its applications. Mater Today: Proc 45:2536–9. https://doi.org/10.1016/j.matpr.2020.11.254.

[15] Hojatzadeh S, Sharifzadeh E, Rahimpour F (2023) An EBM based multi-stage mechanical model to predict the time-dependent creep behavior of semi-crystalline polymer nanocomposites. Mech Mater 184:104737. https://doi.org/10.1016/j.mechmat.2023.104737.

[16] Huang J, Zhou J, Liu M (2022) Interphase in polymer nanocomposites. JACS Au 2(2):280–91. https://doi.org/10.1021/jacsau.1c00430.

[17] Rostami Z, Heidari N, Rahimi M, Azimi N (2022) Enhancing the thermal performance of a photovoltaic panel using nano-graphite/paraffin composite as phase change material. J Therm Anal Calorim 147(5):3947–64. https://doi.org/10.1007/s10973-021-10726-1.

[18] Ghadami H, Sharifzadeh E, Azimi N (2024) A scaling theory to approximate the thermal conductivity of the interphase region in polymer nanocomposites. J Reinf Plast Compos 43(15-16):833–42. 10.1177/07316844231197266.

[19] Azimi N, Sharifzadeh E (2025) Using binary-eutectic phase change materials and ZnO/aluminum nitride nanofillers to improve photovoltaic efficiency. Sol Energy Mater 284:113490. https://doi.org/10.1016/j.solmat.2025.113490.

[20] Sharifzadeh E, Azimi N, Zamanian-Fard A, Mohammadi R (2023) An energy-based strategy to predict the thickness and content of randomly oriented nanolayers aggregates/agglomerates in thermoplastic polymer nanocomposites: experimental and analytical approaches. Polym Sci Eng 63(9):2733–44. https://doi.org/10.1002/pen.26401.

[21] Khanmohammadi S, Azimi N, Sharifzadeh E, Rahimi M, Azimi P (2023) An experimental study to improve cooling on a hot plate using phase change materials and high-frequency ultrasound. J Energy Storage 72:107930. https://doi.org/10.1016/j.est.2023.107930.

[22] Hojatzadeh S, Rahimpour F, Sharifzadeh E (2023) A study on the synergetic effects of self/induced crystallization and nanoparticles on the mechanical properties of semi-crystalline polymer nanocomposites: experimental and analytical approaches. Iran Polym J 32(5):543–55. http://doi.org/10.1007/s13726-023-01144-1.

[23] Sharifzadeh E, Azimi N, Mohammadpour AH (2025) Aggregated/agglomerated and dispersed randomly oriented wavy CNTs in electrically conductive polymer nanocomposites: Impact of dispersion quality and polymer/particle interphase. J Mater Res Technol 35:858–68. https://doi.org/10.1016/j.jmrt.2025.01.061.

[24] Fu S, Sun Z, Huang P, Li Y, Hu N (2019) Some basic aspects of polymer nanocomposites: A critical review. Nano Mater Sci 1(1):2–30. https://doi.org/10.1016/j.nanoms.2019.02.006

[25] Sharifzadeh E, Ader F (2025) Aggregation/agglomeration dependent percolation threshold of spherical nanoparticles in electrically conductive polymer nanocomposites. Polym Compos 46(3):2374–89. https://doi.org/10.1002/pc.29111.

[26] Sharifzadeh E, Azimi N, Mohammadi R (2023) Improved thermostimulative shape memory behavior of HDPE/PET immiscible blend-based polymer nanocomposite using amphiphilic Janus nanoparticles. Polym Compos 44(2):1161–74. https://doi.org/10.1002/pc.27161.

[27] Peigney A, Laurent C, Flahaut E, Bacsa R, Rousset A (2001) Specific surface area of carbon nanotubes and bundles of carbon nanotubes. Carbon 39(4):507–14. https://doi.org/10.1016/S0008-6223(00)00155-X.

[28] Bai J (2003) Evidence of the reinforcement role of chemical vapour deposition multi-walled carbon nanotubes in a polymer matrix. Carbon 41(6):1325–8. http://doi.org/10.1016/S0008-6223(03)00034-4.

[29] Ader F, Sharifzadeh E, Azimi N (2023) A novel strategy to predict the tensile strength of polymer/particle interphase based on De Gennes's self-similar carpet theory. Polym Eng Sci 63(10):3353–61. https://doi.org/10.1002/pen.26449.

[30] Rahimi Mir-Azizi Z, Sharifzadeh E, Rahimpour F (2022) Thermal analysis of ZnO/hollow graphene-oxide/polyester complex- and simple-structure nanocomposites: analytical, simulation and experimental approaches. Iran Polym J 31(6):717–27. http://doi.org/10.1007/s13726-022-01032-0.

[31] Azimi N, Sharifzadeh E (2025) Improved aggregation/agglomeration-dependent percolation theory to predict nanoparticle-aided electrical conductivity in polymer nanocomposites: A combination of analytical strategy and artificial neural network. Comput Mater Sci 246:113424. https://doi.org/10.1016/j.commatsci.2024.113424.

[32] Ader F, Sharifzadeh E, Azimi N (2024) Unveiling the impact of percolation phenomenon on the microstructure of polymer nanocomposites based on the combination of scaling and percolation theories. Polym Compos 45(17):16280–92. https://doi.org/10.1002/pc.28905.

[33] Sharifzadeh E, Ader F, Moradi G (2024) Multi-layer structural representation of polymer/particle interphase region based on De Gennes's scaling theory. J Reinf Plast Compos 1(1):1–14. http://doi.org/10.1177/07316844241279685.

[34] Sharifzadeh E (2025) Energy-based characterization of polymer/particle interphase region as piled-up equilibrated molecular layers: The impact of different distribution patterns of adsorption energy. Polym Eng Sci 65(1):384–400. https://doi.org/10.1002/pen.27017.

[35] Ghasemi F, Sharifzadeh E (2026) An innovative analytical approach to define the dynamic electrical conductivity in polymer nanocomposites: The effect of nanoparticle network rearrangement. Comput Mater Sci 262:114384. https://doi.org/10.1016/j.commatsci.2025.114384.

[36] Sharifzadeh E, Mohammadpour AH, Azimi N (2025) Frequency-Dependent Electrical Conductivity in Polymer Nanocomposites Based on the Impacts of Dispersion Quality and Polymer/Particle Interphase. Polym Compos 1(1):1–13. https://doi.org/10.1002/pc.70495.

[37] Mortazavian S, Fatemi A (2015) Effects of fiber orientation and anisotropy on tensile strength and elastic modulus of short fiber reinforced polymer composites. Compos B: Eng 72:116–29. https://doi.org/10.1016/j.compositesb.2014.11.041.

[38] Ghasemi S, Espahbodi A, Gharib N, Zare Y, Rhee KY (2023) A developed Takayanagi model to estimate the tensile modulus and interphase characteristics of polymer nanocellulose composites. Ind Crops Prod 206:117703. https://doi.org/10.1016/j.indcrop.2023.117703

[39] Bhuiyan MA, Pucha RV, Karevan M, Kalaitzidou K (2011) Tensile modulus of carbon nanotube/polypropylene composites–A computational study based on experimental characterization. Comput Mater Sci 50(8):2347–53. https://doi.org/10.1016/j.commatsci.2011.03.009.

[40] Feng J, Safaei B, Qin Z, Chu F (2023) Nature-inspired energy dissipation sandwich composites reinforced with high-friction graphene. Compos Sci Technol 233:109925. https://doi.org/10.1016/j.compscitech.2023.109925.

[41] Alhijazi M, Safaei B, Zeeshan Q, Asmael M, Harb M, Qin Z (2022) An experimental and metamodeling approach to tensile properties of natural fibers composites. J Polym Environ 30(10):4377–93. https://doi.org/10.1007/s10924-022-02514-1.

[42] Hojatzadeh S, Rahimpour F, Sharifzadeh E (2024) Isothermal crystallization kinetics of pure and surface-modified silica/high-density polyethylene nanocomposites. Polym Compos 45(4):3724–37. https://doi.org/10.1002/pc.28024.

[43] Pyzer-Knapp EO, Pitera JW, Staar PW, Takeda S, Laino T, Sanders DP, et al. (2022) Accelerating materials discovery using artificial intelligence, high performance computing and robotics. npj Comput Mater 8(1):84. https://doi.org/10.1038/s41524-022-00765-z.

[44] Cheetham AK, Seshadri R (2024) Artificial intelligence driving materials discovery? perspective on the article: Scaling deep learning for materials discovery. Chem Mater 36(8):3490–5. https://doi.org/10.1021/acs.chemmater.4c00643.

[45] Shah V, Zadourian S, Yang C, Zhang Z, Gu GX (2022) Data-driven approach for the prediction of mechanical properties of carbon fiber reinforced composites. Mater Adv 3(19):7319–27. 10.1039/D2MA00698G

[46] Béji H, Kanit T, Messager T (2023) Prediction of Effective Elastic and Thermal Properties of Heterogeneous Materials Using Convolutional Neural Networks. Appl Mech 4(1):287–303. https://doi.org/10.3390/applmech4010016.

[47] Champa-Bujaico E, Díez-Pascual AM, Redondo AL, Garcia-Diaz P (2024) Optimization of mechanical properties of multiscale hybrid polymer nanocomposites: A combination of experimental and machine learning techniques. Compos B Eng 269:111099. https://doi.org/10.1016/j.compositesb.2023.111099.

[48] Rajaee P, Rabiee AH, Ashenai Ghasemi F, Fasihi M, Mahabadifar M, Nedaei Shekarab M (2024) XGBoost machine learning assisted prediction of the mechanical and fracture properties of unvulcanized and dynamically vulcanized PP/EPDM reinforced with clay and halloysite nanoparticles. Polym Compos 45(16):14799–815. https://doi.org/10.1002/pc.28801.

[49] Sharma H, Arora G, Kumar R, Debnath S, Siengchin S (2025) Data-driven insights into the high-temperature behavior of polymer/carbon nanotubes nanocomposites. Iran Polym J. http://doi.org/10.1007/s13726-025-01558-z.

[50] Ho NX, Le T-T, Le MV (2022) Development of artificial intelligence based model for the prediction of Young's modulus of polymer/carbon-nanotubes composites. Mech Adv Mater Struct 29(27):5965–78. http://doi.org/10.1080/15376494.2021.1969709.

[51] Le T-T (2021) Prediction of tensile strength of polymer carbon nanotube composites using practical machine learning method. J Compos Mater 55(6):787–811. http://doi.org/10.1177/0021998320953540.

[52] Bhuiyan MA, Pucha RV, Worthy J, Karevan M, Kalaitzidou K (2013) Defining the lower and upper limit of the effective modulus of CNT/polypropylene composites through integration of modeling and experiments. Compos Struct 95:80–7. https://doi.org/10.1016/j.compstruct.2012.06.025.

[53] Makireddi S, Shivaprasad S, Kosuri G, Varghese FV, Balasubramaniam K (2015) Electro-elastic and piezoresistive behavior of flexible MWCNT/PMMA nanocomposite films prepared by solvent casting method for structural health monitoring applications. Compos Sci Technol 118:101–7. https://doi.org/10.1016/j.compscitech.2015.08.014.

[54] Ji XL, Jing JK, Jiang W, Jiang BZ (2002) Tensile modulus of polymer nanocomposites. Polym Sci Eng 42(5):983–93. https://doi.org/10.1002/pen.11007.

[55] Zare Y, Rhee K (2020) A simple technique for calculation of an interphase parameter and interphase modulus for multilayered interphase region in polymer nanocomposites via modeling of young's modulus. Phys Mesomech 23(4):332–9. https://doi.org/10.1134/S1029959920040074.

[56] Yanovsky YG, Kozlov G, Karnet YN (2013) Fractal description of significant nano-effects in polymer composites with nanosized fillers. Aggregation, phase interaction, and reinforcement. Phys Mesomech 16(1):9–22. https://doi.org/10.1134/S1029959913010025.

[57] Treacy MMJ, Ebbesen TW, Gibson JM (1996) Exceptionally high Young's modulus observed for individual carbon

nanotubes. Nature 381(6584):678–80. http://doi.org/10.1038/381678a0.

[58] Wong EW, Sheehan PE, Lieber CM (1997) Nanobeam Mechanics: Elasticity, Strength, and Toughness of Nanorods and Nanotubes. Science 277(5334):1971–5. http://doi.org/10.1126/science.277.5334.1971.

[59] Salvetat-Delmotte J-P, Rubio A (2002) Mechanical properties of carbon nanotubes: a fiber digest for beginners. Carbon 40(10):1729–34. https://doi.org/10.1016/S0008-6223(02)00012-X.